



Research Paper

Carbon-supported $Pd_{100-x}Au_x$ alloy nanoparticles for the electrocatalytic oxidation of formic acid: Influence of metal particles composition on activity enhancement

T. Szumełda, A. Drelinkiewicz*, E. Lalik, R. Kosydar, D. Duraczyńska, J. Gurgul

Jerzy Haber Institute of Catalysis and Surface Chemistry, Polish Academy of Sciences, Niezapominajek 8, 30-239 Krakow, Poland



ARTICLE INFO

Keywords:
 Bimetallic nanoparticles
 Palladium-gold
 Electrocatalytic activity
 Formic acid oxidation

ABSTRACT

Two series of carbon-supported $Pd_{100-x}Au_x$ catalysts of different Au contents have been synthesized by the “water-in-oil” microemulsion method (Triton X 114, cyclohexane) using precursor solutions of low (series L) and high concentration (series H). The metal nanoparticles are characterized by XRD, electron microscopy (SEM, HRTEM) and XPS to determine their crystal structure, particles size, composition and morphology. The electrochemical measurements provide data concerning surface properties of the PdAu particles, including surface fraction of Pd and Au and the reactivity towards hydrogen sorption/desorption processes. The metal particles of low bulk Au-content ($Au/Pd < 1$) are of high monodispersity and of smaller size than their monometallic Pd and Au counterparts, synthesized by the same method. At higher bulk Au-content ($Au/Pd > 1$), the particle size increases approaching almost the size of Au particles. An enrichment of Pd toward the surface of all the $Pd_{100-x}Au_x$ particles occurs, much pronounced in the samples H series. The activity of catalysts (based on the current densities, and TOF values) in the electrooxidation of formic acid (FA) is correlated with the bulk and surface composition of the $Pd_{100-x}Au_x$ particles. The high monodispersity of the metal particle size in the studied catalysts made it possible to observe relation between FA electrooxidation activity and surface composition of the PdAu particles. The catalytically active sites formed at the Au surface fraction ca. 0.1–0.12 (Pd 0.9–0.88) display 1.6-times higher activity (TOF) as compared to pure Pd, while higher surface Au fraction strongly reduces activity. The occurrence of electronic modification of Pd by Au in the $Pd_{100-x}Au_x$ particles also results in a reduced hydrogen solubility, accompanied by weaker Pd–H bonds, which might influence the poisoning ability by CO formed through electroreduction of CO_2 , the product of FA oxidation.

1. Introduction

Formic acid (FA) has great potential as an *in situ* source of hydrogen for fuel cells. It offers high energy density, is non-toxic and can be produced by renewable technologies, namely from lignocellulosic biomass. Currently, catalytic and electrocatalytic decomposition of formic acid in the presence of Pd-based catalysts is widely studied as a promising route of hydrogen generation under mild conditions.

The FA chemical decomposition carried out in vapor or liquid-phase and related electrochemical reaction can proceed via two alternative reaction pathways, dependent on the nature of metal sites; first, the desirable dehydrogenation to hydrogen and carbon dioxide, either $HCOOH \rightarrow CO_2 + H_2$ or $HCOOH \rightarrow CO_2 + 2H^+ + 2e^-$ Eq. (1), and second, the undesirable dehydration to carbon monoxide, $HCOOH \rightarrow CO + H_2O$ Eq. (2), a poison for Pd, Pt [1]. Current research has suggested that Pd is one of the most active catalyst for FA (electro)

chemical decomposition as the direct pathway predominates on Pd-surface, consistent with the DFT calculations [2]. Unfortunately, deactivation of Pd catalysts is commonly observed, caused either by oxidation of Pd surfaces or its poisoning by adsorption of either CO or other unidentified organic species present in the FA fuel [1,3,4]. The spectroscopic studies revealed that $CO_{(ads)}$ accumulated on Pd electrode surface was formed via electrochemical reduction of CO_2 produced in the desired dehydrogenation pathway [5,6]. Such “self-poisoning” mechanism has been proved using electrocatalyst with thin Pd layers deposited on Au substrate [7].

However, Pd-based alloy catalysts offered better performance compared to pure Pd, related to higher resistance to poisoning species. Various bimetallic catalysts such as PdCu, PdPb, PdPt, PdSn, PdCo, PdIr, PdRu, PdNi have been already tested [1]. Among them, the PdAu catalyst has been shown to be one of the most promising catalyst for hydrogen generation via the FA electro(chemical) decomposition.

* corresponding author.

E-mail address: ncdrelin@cyf-kr.edu.pl (A. Drelinkiewicz).

Recently published experimental and calculation studies demonstrated that activity of Pd–Au systems for FA decomposition through a desired dehydrogenation reaction is rationalized either by the “ensemble” effect or the “ligand” effect. The former manifests itself by the appropriate Pd/Au surface atomic arrangements, the latter by the electronic interaction between the Pd surface atoms and atoms (Pd, Au) in the subsurface layer [8]. The existence of electron-rich Pd species in the Pd@Au [9,10] and Pd@Ag [11] core–shell nanostructures enhanced activity as they can weaken the adsorptive strengths of reaction intermediates thus facilitating the O–H and C–H bond cleavage in the Pd–formate intermediates. Furthermore, enhanced tolerance toward CO adsorption observed in numerous FA electrooxidation reactions on the Pd–Au catalysts has been explained by much weaker CO adsorption on Au–surface than on Pd–surface.

An Au-promotion effect was observed using the Pd–Au (electro)catalyst of various configurations including core–shell structures, nanostructured systems, unsupported and carbon-supported PdAu particles. They were prepared by deposition of Pd shells of various thickness on hollow Au nanospheres [12,13], successive deposition of Pd onto Au particles [14] or by a subsequent deposition of Au on the Pd particles in PdAu/MWCNT catalysts [15]. The PdAu nanostructures obtained by typical preparation procedure e.g. co-reduction of Pd and Au precursors carried out at various conditions including different reducing agents and reaction medium (ethylene glycol and sodium citrate medium, THF–water instead of water medium) were also studied [16–21]. Alloying degree of Pd and Au components in these systems was observed to be decisive for the FA electrooxidation activity. The CNT-supported Pd₈₂Au₁₈ particles of alloy structure exhibited higher activity than non–alloy samples or pure Pd [17,18]. Zhang et al. [19] also observed that activity of Pd₈₈Au₁₂/C catalyst with metal particles of high alloying degree prepared in the THF–H₂O mixture displayed higher activity than their counterparts of low alloying degree obtained in aqueous solution. Maiyalagan et al. [20] reported that electroactivity of functionalized graphene-supported Pd_{100–x}Au_x particles increased with growing bulk Au content, but not linearly, the Pd₃Au composition generated the highest electroactivity. For series of f–MWCNT-supported Pd_{100–x}Au_x nanostructured catalysts, the activity dependence on bulk composition was bell-shaped, with maximum attained at the Pd₈₈Au₁₂ bulk composition [21].

In all these studies the activity has been related to bulk Au content in the PdAu structures in spite of the fact that surface properties like Pd/Au ratio and the arrangement of atoms (Pd, Au) are crucial for the electro(chemical) FA decomposition reaction. The identity of the metal atoms adjacent to the Pd atoms at Pd–Au surface was found to be decisive for the directing the FA decomposition via dehydrogenation or dehydration pathways [22]. Pd atoms that reside at Pd–Au interface sites favors FA decomposition through a desired dehydrogenation reaction pathway, whereas Pd atoms which lack neighboring Au atoms, favor dehydration of FA generating CO. It has been also showed by DFT that on the PdAu surface with the reduced amounts of Pd atomic ensembles consisting of three continuous Pd atoms the formation rate of CO can be suppressed because of very high activation energy barrier. [23]. According to Lee et al. [8] the Pd/Au atoms arrangements near the surface is crucial for the reactivity toward FA dehydrogenation path. Among four different PdAu model alloys of different surface and subsurface atomic Pd/Au arrangements, the Pd₃Au₁ was found to be the most preferred as it exhibited the lowest reaction energy barrier for FA dehydrogenation reaction.

However, the controllability over the size and composition of the catalyst particles in most of previous studies have been rather limited because of the choice of the synthesis method. Commonly applied the co-impregnation and subsequent deposition methods produce bimetallic particles of a broad size distribution and the high temperature treatment needed to obtain the alloy structures further facilitates particles aggregation. An alternative are the colloid-based procedures, allowing a better control of the nanoparticles size and composition,

among them the reverse “water-in-oil” microemulsion (w/o) method. This method has attracted much attention for preparation of highly monodisperse particles of metal oxides, metal sulfides, polymers, supported monometallic (Pd, Pt) and bimetallic (PtRu, PtCo, PtAu, PtNi, PdAu, PdPt, AuAg) catalysts [24–27].

In the w/o method the formation of metal particles occurs inside the aqueous droplets acting as individual nano-reactors. As the result, it is possible to (i) control the metal particle size, (ii) obtain a narrow size distribution of metal particles (so-called “monodisperse particles”) thereby allowing high uniformity of their structural and surface properties. The concentration of metal precursor and microemulsion composition are experimental variables playing decisive role in the size, morphology and metal components segregation in the bimetallic particles [27–29]. The formation of metal particles inside the reverse micelles proceeds via nucleation and growth processes. Metal particles are formed from nucleus, which can grow by building up new layers deposited over the previous one. The results of Monte Carlo simulations [28,30] showed that metal components distribution in final particle is defined by a sequence in metal components deposition and the key factor is the difference in their reduction rates mostly governed by a difference in the standard reduction potentials. The metal species having the higher redox potential will precipitate first forming core, followed by the co-precipitation of the second component, which prevails at the surface. The simulated metal components segregation profiles found well confirmation for various experimentally prepared bimetallic nanoparticles [27]. For example, a relatively large difference of the Pd and Au redox potential (AuCl₄[–]/Au 1.00 V and PdCl₄^{2–}/Pd 0.68 V vs SHE) preferred segregation of metal components generating the PdAu nanoclusters with Pd-rich surface [31]. It follows, that the segregation of metal components may be controlled by changing the concentration of metal precursors solution and/or by altering the water/surfactant ratio (parameter *W*). Such possibility has been not only predicted by calculations, but also confirmed by experimental data for the Pt–Au particles [27,29]. In diluted precursors solution almost homogeneous Pt–Au alloy structure was formed, while more concentrated solution promoted surface segregation of Pt [29].

In the present work, two series of carbon-supported catalysts with monodisperse Pd_{100–x}Au_x alloy nanoparticles (from Pd₉₁Au₉ up to Pd₃₆Au₆₄) were prepared by the reverse “water-in-oil” microemulsion procedure, described in detail in our previous papers [32,33]. Keeping the microemulsions composition fixed (Pd/Au ratio) the precursor solutions of low and high concentrations were used to prepare series (L) and (H) catalysts, respectively. Several techniques have been used, namely: XRD, XPS and electron microscopy, to characterize physico-chemical properties of nanoparticles, like their size, morphology, structure and composition. The electrochemical measurements provided data concerning surface properties of the PdAu particles, including surface fraction of Pd and Au components and the reactivity towards hydrogen sorption/desorption processes. The high monodispersity of the metal particle size in the studied catalysts made it possible to found the correlation between the bulk and surface composition of the PdAu/C catalysts and their activity for the FA electro-oxidation. Due to a low Pd loading (2 wt%) in the studied catalysts, it was also possible to observe that the Au component reduces hydrogen solubility in the Pd_{100–x}Au_x particles, compared to pure Pd, as well as that the Pd–H bonds formed in the PdAu alloys are weaker. This may possibly reduce the poisoning effect of CO formed in a side reaction of electroreduction of CO₂.

2. Experimental

Carbon (Vulcan XC72, supplied by CABOT) was used as the support. The catalysts are prepared by means of reverse “water-in-oil” microemulsion method as described in detail in our earlier paper [32]. All the PdAu/C catalysts are synthesized to have Pd loading equal to 2 wt% whereas the Au loading varies resulting in the molar ratio of Pd/Au

from 1: 0.1 up to 1: 1.8. The catalysts are abbreviated as PdAu-X, where X represents the number of Au moles per 1 mol of Pd. Two series of catalysts are prepared. The catalysts of series (L) (abbreviated as PdAu-X/C-L) are prepared using diluted (0.02 M) precursor solution while the precursor solution of 10-times higher concentration (0.2 M) is used to prepare the catalyst of series (H) (abbreviated as PdAu-X/C-H). The 2% Pd/C and 2%Au/C are also prepared using the same preparation procedure.

The reverse micellar solutions are prepared using polyoxyethylene (7–8)octylphenyl ether (Triton-X 114) (Aldrich) as the surfactant and cyclohexane (Aldrich) as the oil phase. In all preparations parameter W (molar ratio of water to surfactant) equal to 5.5 is used. The aqueous solutions of PdCl_2 (molar ratio of NaCl : PdCl_2 = 2, Pd^{2+} ions concentration of 0.2 or 0.02 mol/dm³) and HAuCl_4 commercial reagent (Aldrich) are used as the precursors. NaBH_4 (reagent grade 98%, Aldrich) is used as reducing agent.

In order to prepare 1 g of 2%Pd/C catalyst, 0.94 cm³ of PdCl_2 solution was added to 16.8 cm³ cyclohexane solution of surfactant (0.62 mol/dm³) and the obtained suspension was vigorously stirred up to the formation of a transparent, dark orange solution. In the preparation of PdAu-0.1/C-(H) catalyst, a mixture of PdCl_2 and HAuCl_4 precursor solutions of appropriate volume ratio and the cyclohexane solution of higher surfactant concentration giving the parameter $W = 5.5$ were used. The reducing agent (NaBH_4) was added directly to the microemulsion (molar ration of NaBH_4 to metal ions equal to 10). The color of the liquid quickly changed to black and stirring was continued for another 1 h. Then, the carbon support (0.98 g) was introduced and the system was kept under stirring for 1 h. Deposition of metal nanoparticles on the support was carried out by introducing the THF solvent at a very slow rate, 0.25 cm³/min with an automatic syringe pump. The system was vigorously stirred. The volume of THF added was 3–4 times the volume of the microemulsion. Upon addition of THF, the color of liquid gradually changed from black to gray and finally the liquid became colorless. The catalyst was separated by filtration, dried in air for ca. 24 h and washed with copious amount of methanol and acetone six times and filtrated in between. Finally, the catalysts were washed up with water to remove chloride ions, dried overnight in air and then at 120 °C for 16 h. The Pd/Au ratio of the catalysts was controlled by using the appropriate volume ratio of the precursor solutions. The catalyst PdAu-0.35/C – 2.5 was prepared according to the procedure (H), using a microemulsion of parameter $W = 2.5$.

2.1. Methods of characterization

The X-ray diffraction (XRD) patterns were obtained with a Philips X'PERT diffractometer using $\text{Cu K}\alpha$ radiation (40 kV, 30 mA). The average diameter of metal crystallites was calculated on the basis of the Pd (111) peak broadening according to Scherrer equation.

The X-ray Photoelectron Spectroscopy (XPS) measurements were carried out with a hemispherical analyzer (SES R4000, Gammadata Scienta). The unmonochromatized $\text{Mg K}\alpha$ X-ray source with the anode operating at 12 kV and 20 mA current emission was applied to generate core excitation. All binding energy values were corrected to the carbon C 1s excitation at 285.0 eV. The samples were pressed into indium foil and mounted on a holder. All spectra were collected at pass energy of 100 eV except the survey scans which were collected at pass energy of 200 eV. Intensities were estimated by calculating the integral of each peak, after subtraction of the Shirley-type background, and fitting the experimental curve with a combination of Gaussian and Lorentzian lines of variable proportions (70:30).

Electron Microscopy (SEM) studies were performed by means of Field Emission Scanning Electron Microscope JEOL JSM – 7500F equipped with the X-ray energy dispersive (EDS) system. The secondary electron detector provided SEI images, and back scattered electron detector provided BSE (COMPO) micrographs.

To prepare the particle size distribution diagram at least 100 particles (N) were manually counted. The counting was carried out on electron micrographs registered at 100000–200000 magnifications, where metal particles very well contrasted with the carbon material and they were clearly detected. On these micrographs registered in BSE (COMPO) mode the accuracy of the particle size scale was 0.5 nm.

HRTEM and STEM studies were performed on FEI Tecnai G² transmission electron microscope operating at 200 kV equipped with EDAX EDX and HAADF/STEM detectors. Samples for analysis were prepared by placing a drop of the suspension of sample in ethanol or THF onto a carbon-coated copper grid, followed by evaporating the solvent. The local composition of the metal particles was determined by energy dispersive X-ray emission (EDX). The spatial resolution of analysis is as high as 1.5 nm so that the composition of individual particles can be measured.

2.2. Electrochemical measurements

Electrochemical measurements have been performed in a conventional three electrode electrochemical cell using a CH Instrument (Austin, TX, USA) Model 760D workstation. A graphite rod and a mercury/mercury sulfate electrode ($\text{Hg}/\text{Hg}_2\text{SO}_4$, 0.718 V vs reversible hydrogen electrode), were used as the counter electrode and the reference electrode, respectively. A glassy carbon disk electrode (GC) (2.805 mm radius, geometric area, 0.247 cm²) was used as the working electrode. The ink of carbon-supported catalysts was prepared by ultrasonically mixing 5 mg of catalyst sample with 0.029 cm³ of Nafion (5 wt.% in lower aliphatic alcohols and water, Aldrich) in 1 cm³ of 2-propanol solution. 13.3 μl of the suspension was dropped onto the GC electrode by a microsyringe and left to dry (ca. 30 min) at room temperature (corresponds to constant Pd loading on the electrode 10 $\mu\text{g}/\text{cm}^2$). All electrochemical experiments were performed in an Ar deoxygenated solution at a scan rate of 50 mV/s at room temperature and ambient pressure, employing 0.5 M sulfuric acid as the electrolyte solution. Studies of formic acid electrooxidation were performed in 0.5 M sulfuric acid containing 0.5 M formic acid (96% ACS Reagent Grade, Aldrich). The potentials values mentioned in the text are referred to reversible hydrogen electrode RHE.

The metal dispersion (D) in catalysts was calculated using the formula [33]

$$D = \frac{6 \cdot n_s \cdot M}{\rho \cdot N_A \cdot d_{av}} \quad (1)$$

where

M – is the molecular weight, N_A is $6.023 \times 10^{23} \text{ mol}^{-1}$
 n_s is the number of atoms at the surface per unit area [$n_s(\text{Pd}) = 1.27 \cdot 10^{19} \text{ m}^{-2}$, $n_s(\text{Au}) = 1.15 \cdot 10^{19} \text{ m}^{-2}$]
 ρ is the density ($\rho_{\text{Pd}} = 1.20 \cdot 10^7 \text{ g/m}^3$, $\rho_{\text{Au}} = 1.95 \cdot 10^7 \text{ g/m}^3$)
 d_{av} is the average particle size measured by XRD/SEM

For the bimetallic catalysts, the average numbers of the parameters n_s and ρ were calculated to obtain the metal dispersion considering the actual Pd/Au composition

3. Results and discussion

3.1. Physicochemical characterization of the catalysts

3.1.1. XRD studies

To determine the morphological and structural characteristics of bimetallic $\text{Pd}_{100-x}\text{Au}_x$ nanoparticles with varying Au content the catalysts are characterized by powder XRD. The XRD patterns of the Pd/C, PdAu-0.8/C(H) catalysts and carbon support are displayed in Fig. 1a. The pattern of carbon support shows a broad reflection centered at $2\theta = 43\text{--}44^\circ$ arising from a hexagonal structure of Vulcan XC 72 carbon. The patterns of both catalysts show reflections characteristic of a face-centered-cubic (fcc) lattice, corresponding to the structures of Pd

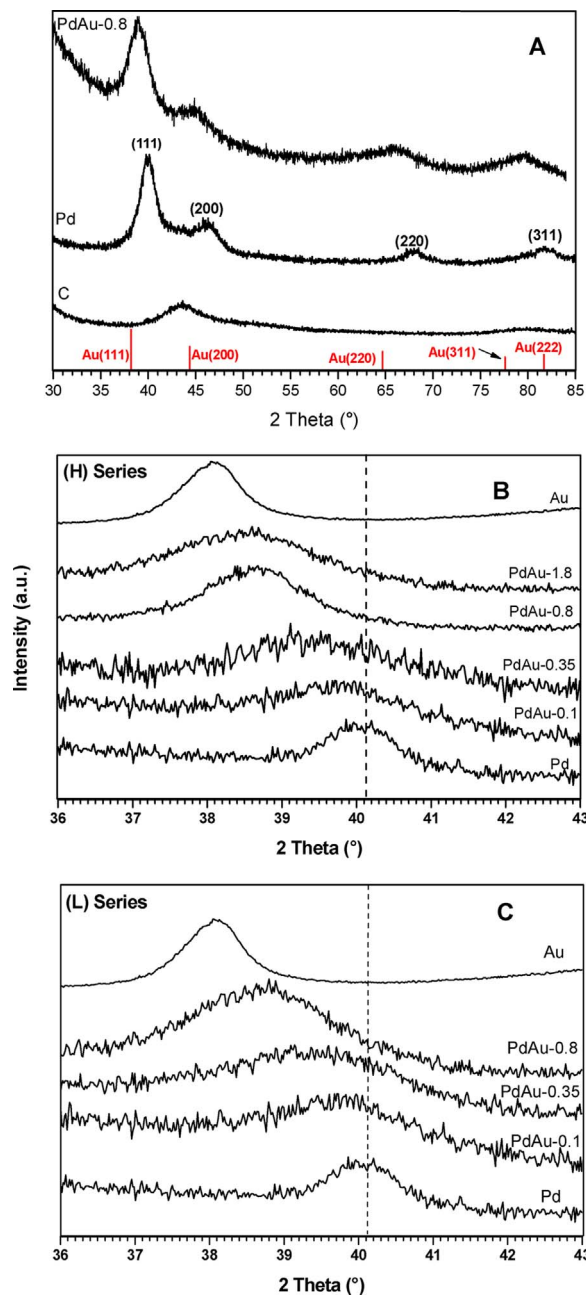


Fig. 1. XRD diffraction patterns of carbon support, Pd/C and PdAu-0.8/C(H) catalysts, the reflections of the fcc crystal structure of Au are indicated (a); the 20 range of (111) reflection in patterns of (H) series (b) and (L) series PdAu/C (c) catalysts.

or PdAu crystallites. The reflections of PdAu-0.8 crystallites are shifted to lower angles compared to those of Pd, indicating an increased lattice parameter due to the alloying of Pd with Au. Figs. 1b and 1c demonstrate a gradual expansion of PdAu lattice with increasing bulk Au content in the $Pd_{100-x}Au_x$ particles of both series (H) and (L), evident from the Pd(111) reflection shifted continually from the original 20 of 40.07° in the Pd/C toward the 20 of 38.12° observed for the Au/C catalyst. The lattice parameter “a” increases with the bulk Au content in similar manner for both series (H) and (L) (Fig. 2). The increase appears to be linear up to the Au/Pd ratio approaching unity, at which point an upward deviation from linearity can be observed. This seems to indicate that at the Au/Pd ratio exceeding unity, the nanoparticles no longer retain the alloy structure [34]. Rather than being mixed homogeneously at atomic level, they consist of a mixture of Au crystallites with certain contribution of the Pd-Au alloy structure. Similar variation

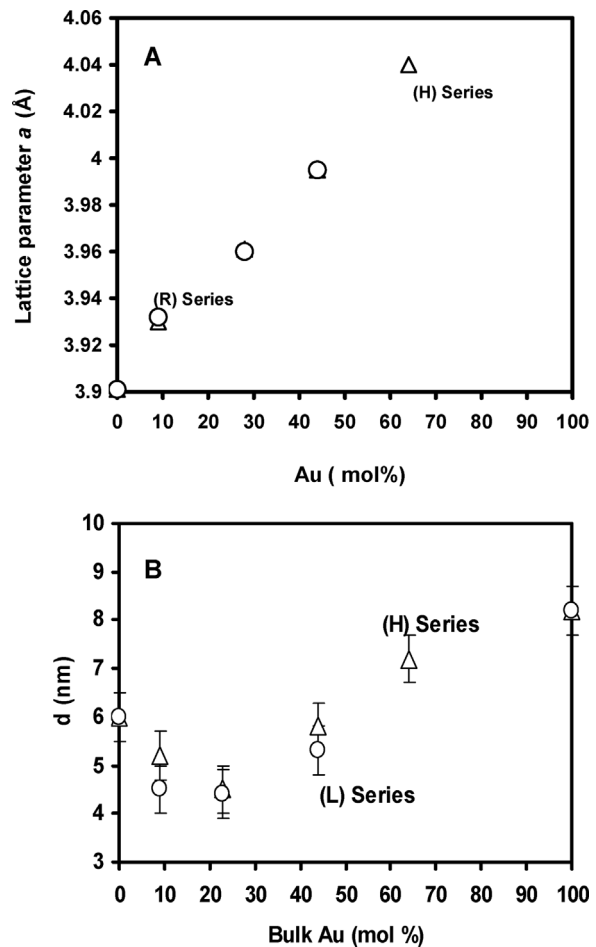


Fig. 2. The lattice parameter “a” and the average size of metal crystallites “d” as a function of the Au bulk content in the PdAu/C catalysts.

of the PdAu alloy structure at the bulk Au fraction above 0.6 was reported for series of $Pd_{100-x}Au_x/Al_2O_3$ catalysts with metal particles of ca. 10 nm, prepared by co-impregnation followed by hydrazine reduction at room temperature [35].

The average metal crystallite size in studied catalysts calculated from the broadening of the metal (111) line using Scherrer equation are collected in Table 1. A change of metal crystallite size with the bulk Au content is reported in Fig. 2.

3.1.2. Electron microscopy studies (SEM, TEM, HRTEM)

The representative TEM micrographs of catalysts are displayed in Fig. 3. Fig. S1 presents the SEM images of monometallic Pd/C, Au/C and bimetallic PdAu/C catalysts. Similarly to our previous results dealing with carbon-supported PdAu catalysts [32] finely dispersed metal particles, Pd and bimetallic ones can be seen in the studied catalysts. The Pd/Au atomic ratios determined by the EDS analysis (Table 1) agree well with the nominal composition intended in preparation, evidencing effective deposition of both metal components on the carbon support. The metal particles, in the Pd/C and PdAu/C catalysts all are spherically shaped, with individual nanoparticles strongly predominating over occasionally formed small aggregates. The aggregated particles were omitted in the preparation of particle size distribution profiles. The particles size distribution diagrams (Fig. 4) show high monodispersity of both the monometallic Pd as well as the bimetallic PdAu particles of low Au content. The particle size distributions for the Au/C and the Au-rich PdAu-1.8/C catalysts are broader. In the Au-rich catalyst, the particles are of relatively large size (7.2 nm) close to that of pure Au (8.2 nm). Moreover, as shown in Fig. 2, a

Table 1

Physicochemical characterization of studied catalysts and their activity in the formic acid electrooxidation.

Catalyst/preparation	Metal particle size d nm	Pd/Au atomic ratio		Metal dispersion D%	Formic acid electro-oxidation		
		EDS	STEM		EASA m ² /g Pd	I max mA/cm ²	TOF s ⁻¹
Pd	6.0			18.7	15.1	4.73	11.36
PdAu-0.1 (Pd ₉₁ Au ₉)	L	4.5	90/10	87/13	24.2	34.8	6.01
	H	5.2		91/9	21.0	19.7	8.06
PdAu-0.35 (Pd ₇₇ Au ₂₃)	L	4.4	73/27		24.4	15.1	7.41
	H	4.5	75/25	68/32	23.8	15.1	7.36
PdAu-0.35(2.5) (Pd ₇₇ Au ₂₃)	H	4.0	76/24		26.1	7.12	7.60
PdAu-0.8 (Pd ₅₆ Au ₄₄)	L	5.3		54/46	20.3	17.50	5.42
	H	5.8	60/40	55/44	18.6	33.01	0.91
PdAu-1.8 (Pd ₃₆ Au ₆₄)	H	7.2	38/62	37/63	15.1	43.36	0.85
Au		8.2			11.6		1.67

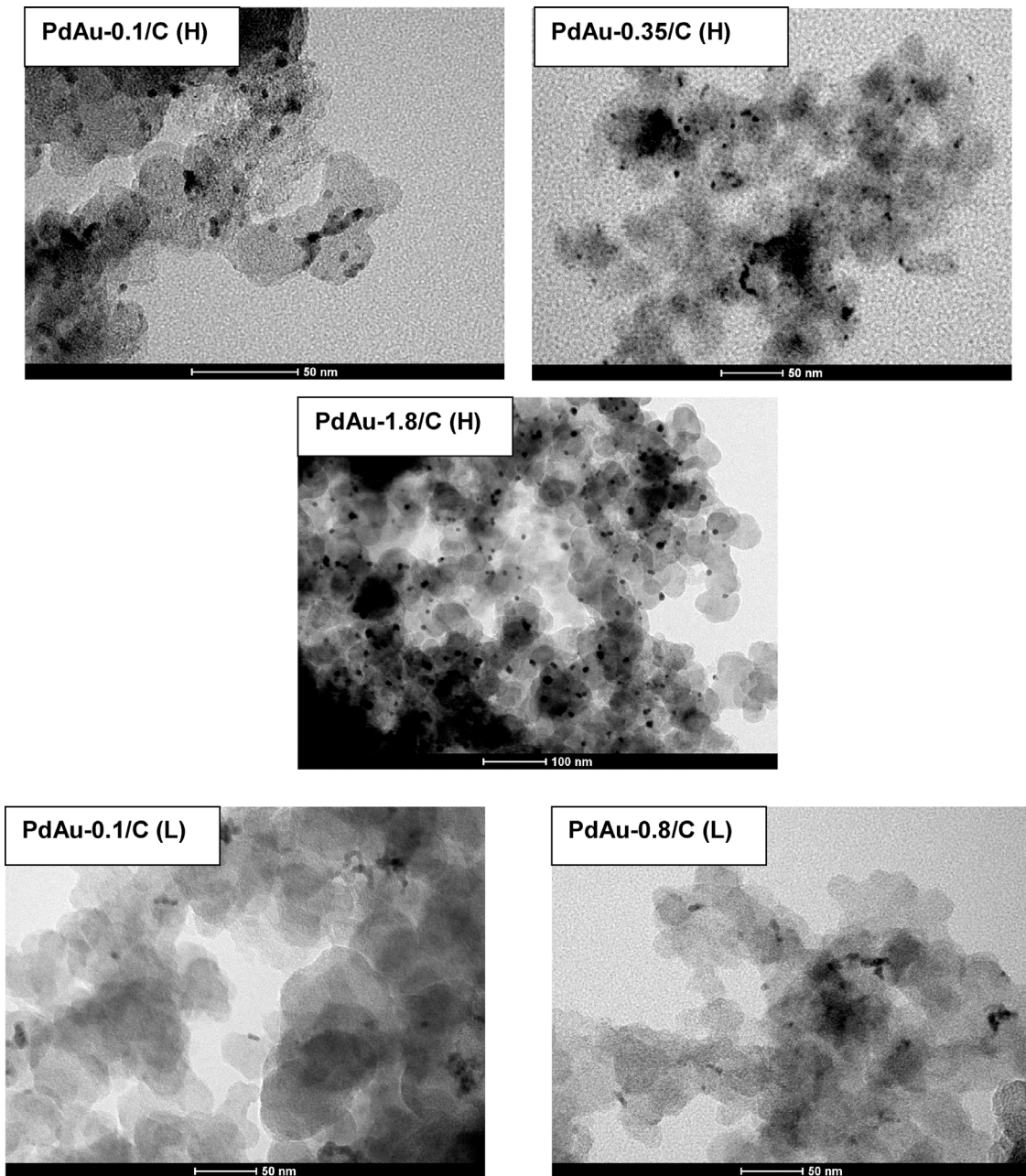


Fig. 3. TEM images of series (H) catalysts: PdAu-0.1/C(H), PdAu-0.35/C(H), PdAu-1.8/C(H) and series (L) catalysts: PdAu-0.1/C(L), PdAu-0.8/C(L).

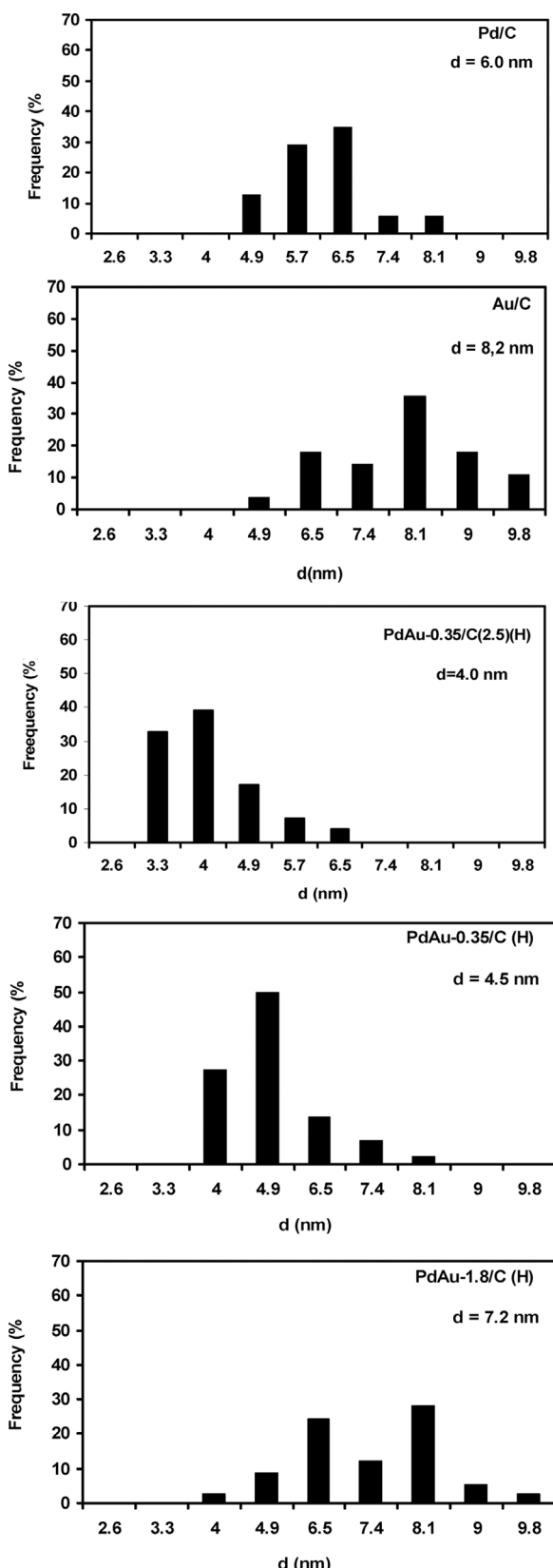


Fig. 4. Metal particle size distribution diagrams for monometallic Pd/C, Au/C and bimetallic PdAu-0.35/C(H), PdAu-0.35($w = 2.5$) and PdAu-1.8/C(H) catalysts.

deviation from linearity for the lattice parameter existed at the PdAu-1.8 composition.

Since SEM-EDS method does not give compositional information

concerning individual particles because the method is restricted in resolution, the selected PdAu catalysts are subjected to the HRTEM studies (Fig. 5, Fig. S2). Morphology and composition of individual particles, chosen randomly, were studied by the STEM attached to a high-resolution HRTEM. Energy-dispersive X-ray analysis (TEM-EDX) was conducted on several different selected individual metal particles on each catalyst. The HRTEM images showed that each individual particle may be considered as a single crystal with crystal lattice spread through the whole particle, indicating the alloy structure of the particles. The STEM analysis (Table 1) confirmed co-existence of both Pd and Au components in all studied catalysts. The obtained average composition of individual particles is close to the nominal composition as intended in the synthesis, albeit with a certain deviation. It might result from very weak detection signal as well as from the detection errors because of relatively low content of metals in studied catalysts.

As shown in Fig. 2 at the Au/Pd ratio below unity, the $Pd_{100-x}Au_x$ crystallites are around 4–5 nm in size, which is lower than either the pure Pd (6.1 nm) or pure Au (8.2 nm) crystallites. This observation is consistent with the literature data for other bimetallic particles PdAu [31], PtAu [36], PtAg [37] and AuAg [38] also prepared by microemulsion procedure. The smaller size of bimetallic particles compared to that of corresponding monometallic ones together with a monodispersity of the bimetallic particles, has been related to a decisive role of nucleation process during the particles formation [36–38].

The data in Fig. 2 show that there is no essential difference between the size of (H) and (L) series PdAu particles. However, at the same bulk Au content, the particles of (H) series prepared in concentrated solution seems to be slightly larger than their counterparts prepared in diluted precursor solution (L). This effect observed in the entire range of bulk Au-content in studied catalysts, is consistent with the Monte Carlo simulations [39] and was observed for the monometallic Pt [40] and bimetallic PtRu particles [41] synthesized also by microemulsion method. In both the Pt and PtRu systems, the size of metal crystallites increased with growing concentration of precursor solutions, however, the relation was not proportional.

3.1.3. XPS studies

The catalysts are also subjected to the X-ray photoelectron spectroscopy (XPS) measurements. The binding energies of Pd 3d_{5/2} and Au 4f_{7/2} are collected in Table 2 and the XPS spectra are displayed in Fig. S 3. It should be pointed out that no chlorine residuals from the metal precursors were found in the XPS survey scan.

The depth of X-ray penetration ca. 6–10 nm makes it difficult to analyze the surface composition of the samples with metal nanoparticles of ca. 4–6 nm in size deposited on support. Nevertheless, the XPS-derived Pd/Au atomic ratio might provide a hint concerning segregation of Pd and Au components in studied catalysts (Table 2). The bulk Pd/Au ratio and those determined by XPS and CV techniques (Section 3.2) all are similar for the PdAu-0.1(L) catalyst only, suggesting a nearly homogeneous distribution of Pd and Au through the particle. For the other catalysts, the XPS and CV-derived Pd/Au ratios are higher than the corresponding bulk compositions indicating Pd-rich surface.

In the spectrum of Pd/C catalyst the Pd 3d_{5/2} peak component at binding energy of 335.55 eV strongly predominates with a small contribution of a peak at 336.42 eV. The first predominating energy is typical for metallic palladium whereas the second higher energy (336.42 eV) is usually attributed to the palladium species of lower electron density compared to Pd-metal or to oxidized palladium like PdO formed due to surface oxidation of palladium particles.

For all bimetallic particles with Pd-rich surface the Pd 3d energy is lower by 0.35–0.5 eV compared to pure Pd, irrespective of bulk Au content. It shows a modification of palladium electronic properties by Au. However, in two Au-rich catalysts PdAu-0.8/C(H) and PdAu-1.8/C(H), with a non-homogenous composition of the surface (Fig. 6), the Pd 3d_{5/2} energy shift is distinctly smaller, by 0.17 eV at PdAu-0.8

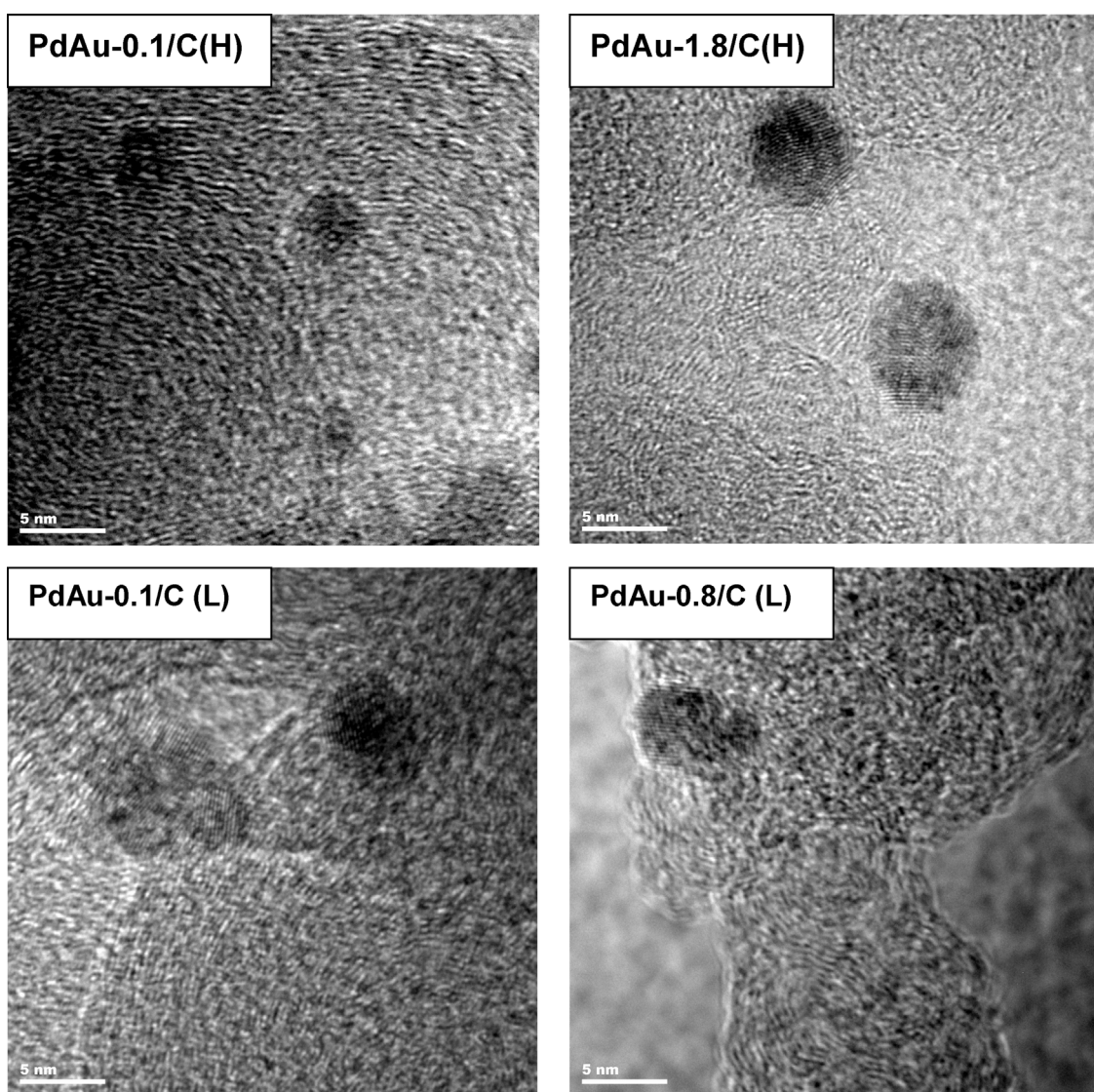


Fig. 5. HRTEM micrographs of PdAu-0.1/C(H), PdAu-1.8/C(H) and PdAu-0.1/C(L), PdAu-0.8/C(L) catalysts.

Table 2
Characterization of catalysts with CV and XPS methods.

Catalyst	E _p (V) ^a	Surface fraction from CV		Pd/Au atomic ratio			XPS BE (eV)	
		Pd	Au	bulk	XPS surface	CV surface	Pd 3d _{5/2}	Au 4f _{7/2}
Pd	H	0.167	1				335.5 0.6	
PdAu-0.1 (Pd ₉₁ Au ₉)	L	0.118	0.91	10	9.3	10.1	336.4 0.4	
	H	0.189	0.97				335.1	83.5
PdAu-0.35 (Pd ₇₇ Au ₂₃)	L	0.138	0.92	3.35		11.5	335.2 0.6	
	H	0.124 ^b	0.93				335.9 0.4	
PdAu-0.35(2.5)	H		0.88	6.0		13.2	335.0	83.2
			0.12					
PdAu-0.8 (Pd ₅₆ Au ₄₄)	L	0.118 ^b	0.76	1.27	1.8	7.33	335.2 0.8	
	H	0.120					336.5 0.2	
PdAu-1.8 (Pd ₃₆ Au ₆₄)	H	No ^c		0.56	1.1	3.16	335.4 0.7	
	H	No ^d					336.3 0.3	
Au			1				335.7	84.2
								84.4

a potential of hydrogen desorption peak.

b hydrogen sorption strongly suppressed.

c hydrogen sorption almost fully suppressed.

d no hydrogen sorption.

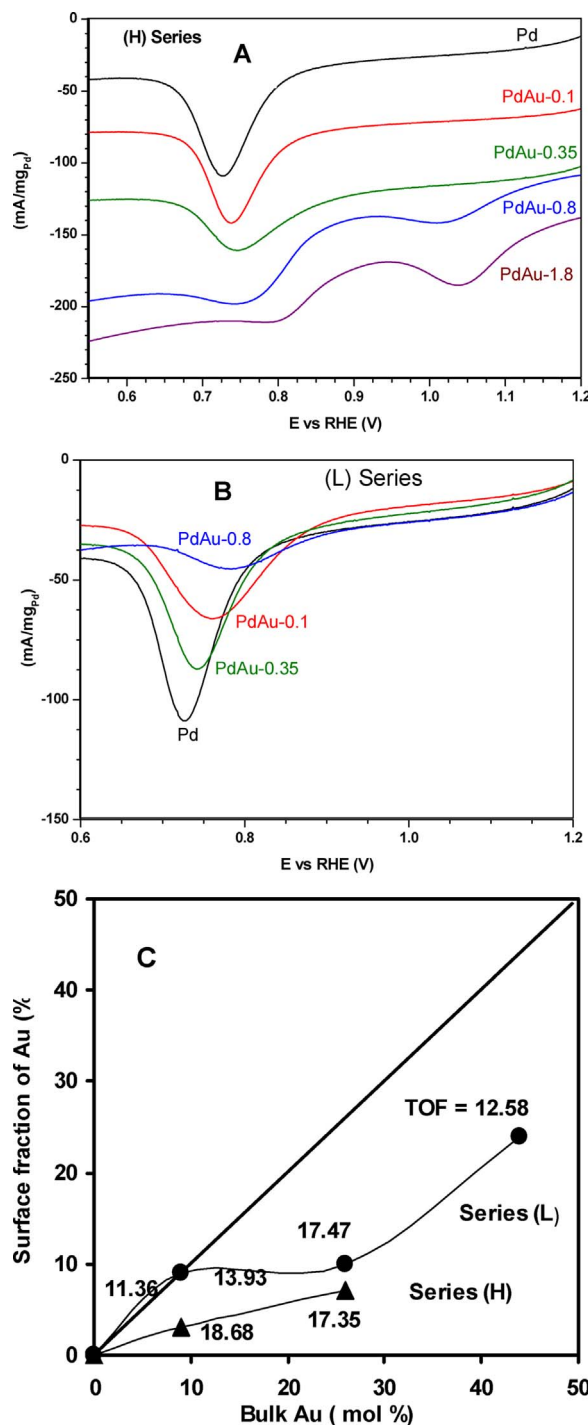


Fig. 6. The magnified view of CV profiles in the potential region (0.6–0.9 V) of surface oxides reduction for Pd/C and bimetallic PdAu/C catalysts of (H) series (a) and (L) series (b) (Ar-saturated 0.5 M H_2SO_4 solution, scan rate of 50 mV/s); Surface Au atomic fraction as a function of the bulk Au content in the PdAu/C catalysts (c).

composition. At PdAu-1.8 composition when bulk Au content is above that of Pd, the observed Pd $3d_{5/2}$ energy 335.70 eV is higher than that in the Pd/C.

3.2. Electrochemical properties of the catalysts

The representative CV profiles registered in 0.5 M H_2SO_4 solution for Pd/C and selected PdAu/C catalysts are displayed in Fig. S 4. The CV profiles of studied catalysts show the well resolved two peaks due to hydrogen absorption/desorption. The magnified view of hydrogen

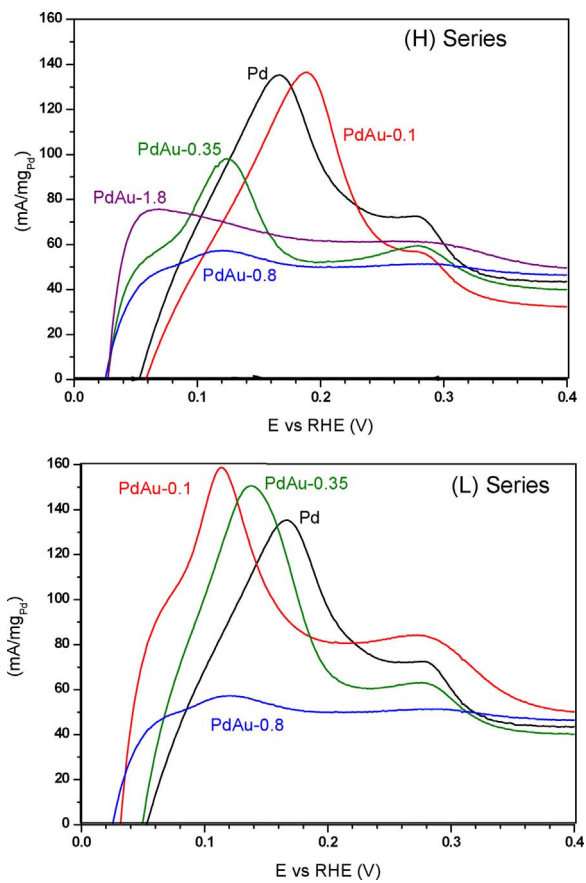


Fig. 7. The magnified view of CV profiles in the potential region of hydrogen desorption (0.0–0.4 V) for PdAu/C catalysts (Ar-saturated 0.5 M H_2SO_4 solution, scan rate of 50 mV/s).

desorption (oxidation) potential region is reported in Fig. 7.

It should be noted that the resolved peaks have been observed for thin Pd films, the Pd nanostructures or Pd nanoparticles e.g. when the contribution of palladium surface is much higher than its volume. In these palladium systems, the current for the formation of absorbed hydrogen does not dominate as it does for massive palladium electrode [42] or electrocatalysts with high Pd loading 20–40 wt% Pd commonly studied for electrooxidation of FA. In the latter case, the hydrogen desorption peak is broad and unresolved because hydrogen adsorbed at the surface represents only a very small fraction of total hydrogen sorbed. Among the two resolved hydrogen desorption peaks, the first at more negative potential (0.1–0.2 V vs RHE), originates mainly from the oxidation of hydrogen from the β -PdH hydride phase. The second peak at more positive potential ca. 0.28 V (vs. RHE) corresponds to the desorption (electrooxidation) of adsorbed hydrogen at the palladium surface.

No hydrogen adsorption/desorption peaks on the 2%Au/C catalyst are observed, consistent with the literature data [43]. The shape of hydrogen desorption peaks and their potentials on PdAu/C catalysts differ from those on pure Pd/C (Fig. 7). The current due to hydrogen desorption peak gradually decreases with growing bulk Au content and at comparable Pd and Au contents at the PdAu-0.8 composition, the hydrogen-desorption peaks are very weak showing a distinct suppression of hydrogen sorption, consistent with the gas-phase hydrogen chemisorption and electrochemical measurements for the PdAu samples [34,43]. It is also observed that with growing bulk Au-content the first hydrogen desorption peak shifts gradually to lower potentials relative to that on pure Pd (Table 2). No essential difference between the potentials for series L and H exists. An exception is the PdAu-0.1/C(H) sample showing slightly higher hydrogen desorption potential.

The gas-phase hydrogen chemisorption experiments and electrochemical measurements showed that alloying palladium with non-hydrogen absorbing gold reduced the ability of palladium to the formation of Pd-hydride phase. Kobayashi et al. [34] observed that the ability of palladium in the PdAu nanoparticles of alloy structure (ca. 8 nm) to the formation of Pd-hydride phase upon sorption of gaseous hydrogen (at 0.1 MPa) decreases with growing Au content. On Pd₈₀Au₂₀ a reduction of more than half of the hydrogen capacity with respect to Pd was observed and the Pd₅₀Au₅₀ nanoparticles hardly absorbed hydrogen (ca. 0.025 H/M). This drastic reduction in hydrogen absorption has been related to a solid-solution type of Pd-Au structure, where Pd and Au atoms are homogeneously mixed at the atomic level. Electrochemically obtained results on limited volume Pd-Au electrodes also indicated that hydrogen capacity decreased with growing amount of Au. The hydrogen capacity 0.75 H/Pd decreased to ca. 0.4 H/M at 30 at% Au and ceased (reached zero) at 60–70 at.% Au in these PdAu films [43]. The reduced capacity of hydrogen was accompanied by a negative shift of the first hydrogen desorption potential [43,44]. The potential shifted especially distinctly at low Au content, by ca. 0.2 V at 20 at% Au whereas the changes were less distinct at further growth of Au content [44]. Similar effect has been observed for thin films of another Pd-based alloys such as PdRh, PdRu [45], Pd-Cu [46] as well as carbon-supported PdPt nanoparticles [47]. More negative potential indicates facilitated removal of hydrogen from these Pd-alloys in comparison with pure Pd related to modification of Pd electronic properties by the added metal (Au, Rh, Pt). Kibler et al. [48] reported that the potential of hydrogen desorption peaks could serve as a measure for the hydrogen bonding strength. For series of palladium monolayers on single-crystal electrodes Au, Pt, Ir, Rh, Ru and Re a linear relation between the potential of hydrogen desorption peak and calculated shift of the d-band center [49] was obtained.

The second hydrogen-desorption peak at more positive potential, ca. 0.28 V (RHE) (Fig. 7) is attributed to the desorption of hydrogen from the metal surface. Although this signal may contain some contribution from a bulk process of the hydride (α -PdH) decomposition, its potential correlated with the surface composition of the PdRh alloys [45]. With growing surface content of Rh the potential shifted negatively relative to that on pure Pd.

As Fig. 7 shows, the potential of second hydrogen desorption peak on PdAu/C catalysts does not remarkably differ from that on Pd which might be related to relatively low surface fraction of Au in these catalysts (Table 2). Thus, similarly to previous reports the strength of hydrogen bonding in our PdAu/C catalysts is weaker than in pure Pd and with growing Au-content the capacity of hydrogen sorbed decreases and the removal of hydrogen becomes more and more easier.

The magnified view of CV profiles in potential region corresponding to the reduction of surface oxides in the PdAu/C catalysts of series (H) and (L) are reported in Fig. 6 a and b, respectively.

The electrochemically active surface area (EASA, cm^2) of the catalysts (Table 1) is determined from the surface oxide reduction charge (Q, mC) and double layer capacity, which is a well-established and generally accepted method in the case of Pd-containing samples. The EASA was estimated using the relation $\text{EASA} = Q/S$, where Q is the observed coulombic charge (mC) and S is the proportionality factor, 0.424 mC/cm^2 corresponding to the reduction of PdO [42,50].

The surface composition of Pd_{100-x}Au_x particles, express as a fraction of Pd and Au, could be estimated from the potential of oxide reduction peak by method reported by Rand [51] which is based on a linear dependence of the potential of surface oxide reduction peak ($E_{\text{P,Alloy}}$) and alloy surface composition:

$$E_{\text{P,Alloy}} = X_{\text{Pd}} E_{\text{P,Pd}} + X_{\text{Au}} E_{\text{P,Au}} \quad (2)$$

where $E_{\text{P,Pd}}$, $E_{\text{P,Au}}$ are the oxide reduction peak potentials for the pure Pd/C and Au/C catalysts and X_{Pd} and X_{Au} are the surface fractions of Pd and Au, respectively. This method has already been applied to

determine surface composition of carbon-supported PdPt/C, PdAu/C and PdPtAu/C catalysts [52,53].

According to Rand [51] in the case of bimetallic systems, a single reduction peak indicates homogeneous composition of the alloy surface. The presence of multiple signals due to surface oxide reduction indicates surface heterogeneity, i.e., the existence of separate “areas” of different compositions.

For PdAu/C catalysts of series (L) a well defined and relatively narrow single surface oxides reduction peaks across the entire range of Au compositions studied, from PdAu-0.1 up to PdAu-0.8 is observed (Fig. 6 b). Their potentials locate between the reduction of Pd (0.73 V, RHE) and Au (1.09 V, RHE) showing that surface of all bimetallic PdAu nanoparticles of series (L) consists of Pd and Au components. Similarly, a single oxide reduction peaks can be seen for the two catalysts of series (H) with low Au content, PdAu-0.1 and PdAu-0.35 (Fig. 6 a). However, for Au-rich catalysts, Pd-Au-0.8/C(H) and Pd-Au-1.8/C(H) two reduction peaks at potential between those of pure Pd and pure Au appear. According to Rand [51] it is result of surface heterogeneity, i.e. the existence of “surface areas” of different Pd/Au compositions. The reduction peak at the lower potential (0.75 vs RHE) could be attributed to Pd-rich “surface area”, the peak at higher potential (1.05 V vs RHE) might originate from Au-rich “surface area”. Similar CV curves showing heterogeneity of Pd-Au surface due to surface areas of different Pd/Au contents have been also reported for the thin films of electrochemically deposited PdAu alloys [44] and for the carbon-supported bimetallic PdAu particles with bulk Au content equal or higher than Pd [52,53].

Surface fractions of Au and Pd calculated from Eq. (2) are summarized in Table 2. For these two Au-rich PdAu-0.8(H) and Pd-Au-1.8(H) catalysts with a complex picture of surface oxide reductions peaks, the surface fraction of Au and Pd are not calculated.

It can be seen that the Pd/Au ratios determined by CV and XPS are similar to the bulk Pd/Au ratio for the PdAu-0.1(L) catalyst only, suggesting a nearly homogeneous distribution of Pd and Au through the particle. For the other catalysts, the XPS and CV-derived Pd/Au ratios are higher than the corresponding bulk compositions indicating Pd-rich surface.

Fig. 6c presents the surface fraction of Au as a function of the bulk Au content in both series catalysts. The solid line in Fig. 6c corresponds to a hypothetical case when the surface and bulk Au contents are equal. It is observed that only at the lowest bulk Au content in PdAu-0.1(L) catalyst, the surface fraction and bulk content of Au are close (9%). The surface fractions of Au are below the corresponding bulk Au contents in all other catalysts. It shows a strong surface segregation of palladium resulting in the Pd-rich outer surface of all the bimetallic PdAu particles. The Au-surface fractions is within the range 0.07–0.09 in the particles of both series when the bulk Au content is much lower compared to that of Pd, e.g up to Pd₇₇Au₂₃ bulk composition. In the PdAu-0.35(2.5) particles with the same bulk composition but smaller average size (4.0 nm, Table 1) the surface Au fraction is only slightly higher, equal to 0.12 (Table 2). However, when the bulk contents of Pd and Au are comparable as at Pd₅₆Au₄₄ composition, the surface of particles prepared in diluted solution [PdAu-0.8(L)] is homogenous with Au fraction of 0.24. On the other hand, preparation in concentrated solution [PdAu-0.8(H)] results in the particles of non-homogeneous surface composition.

Thus, an enrichment of Pd toward the surface of the PdAu particles occurs, similarly to what was observed for the PdAu colloidal particles synthesized by ethanol co-reduction in the presence of protective polymer PVP [54] and upon preparation of the PdAu nanoclusters by means of microemulsion procedure [31]. Metal segregation in these clusters was related to the difference in the reduction potential and, in addition it was also related to the nucleation rates of the metals. Large difference of the Au and Pd reduction potential ($\Delta \varepsilon^0 = 0.39 \text{ V}$) resulted in preferential segregation of Pd to the surface of PdAu colloidal particles [54]. Pd segregation to the surface layer of PdAu clusters prepared by microemulsion procedure was related to a faster nucleation

rate of Au compared to that of Pd [31]. Similarly, much faster nucleation of Au compared to that of Pt or Ag generated bimetallic AgAu and PtAu particles with Ag or Pt – rich surface [37,38].

The obtained data also show that concentration of precursor solution has a distinct impact on the segregation of Pd and Au components especially when the bulk Au content is very low (PdAu-0.1) or comparable to that of Pd (PdAu-0.8). More concentrated precursor solution used in series (H) catalysts results in much stronger surface segregation of Pd generating the PdAu-0.1(H) particles of much smaller Au surface fraction (0.03) than that obtained in its counterpart synthesized in diluted solution (Au fraction of 0.09).

In the two Au-rich catalysts prepared in more concentrated precursor solution, the CV measurements showed non-homogeneous composition of metal particles surface. Areas of various extents of Pd surface enrichment are evidenced by the metal oxide reduction peaks. The morphological (SEM) and structural (XRD) characteristics of the metal particle in the PdAu-1.8/C catalyst (e.g. average crystallite size, a broad distribution of metal particles, lattice parameter does not fit linear relation) suggest that similarly to what was observed for PdAu/Al₂O₃ [35] it is probable that Pd mostly appears in the form of some of surface “Pd-enriched Pd/Au islands” on strongly Au-rich crystalline particles. This surface architecture might explain a different energy effect in the Pd 3d binding energy of PdAu-1.8/C catalyst compared to other catalysts.

Diluted precursor solution in series L preparation, facilitates intermixing of Au and Pd resulting in more homogenous microstructure of the PdAu particles. The observed influence of precursor solution concentration is consisted with the Monte Carlo simulations [27] and experimental results for the PtAu nanoclusters [29]. In diluted precursors solution almost homogeneous PtAu alloy structure was formed, while concentrated precursor solution facilitated segregation process resulting in Pt-rich outer surface of PtAu particles [29].

It should be noticed that the surface fraction of Au within similar range 0.07–0.12 is observed (Table 2) which corresponds to the surface Pd/Au atomic ratio of approximately 9/1. The formation of particles with the surface shell of Pd/Au ~9/1 composition with a consequent enrichment of their core by Au is assisted by smaller size of the bimetallic particles compared to monometallic counterparts (Fig. 2, Table 1). It might be result of much faster nucleation rate of Au compared to Pd although a difference in the reduction potentials of Au and Pd could also contribute to the metal components segregation process.

3.3. Electrochemical oxidation of formic acid

Fig. 8 presents cyclic voltammograms of formic acid (FA) oxidation on PdAu/C catalysts. Similarly to the results reported for the carbon-supported Pd-based bimetallic catalysts [17,21,55,56] through normalizing the currents of FA oxidation by the active surface areas which are calculated on the basis of the peak areas of Pd surface oxide reduction, the Pd-specific activities are obtained. No current due to FA oxidation is observed at the 2% Au/C catalyst indicating that pure Au is inactive and the Au could be considered as an inert additive. The maximum current for the FA oxidation on pure Pd/C is observed at 0.54 V (RHE) which agrees with other authors and corresponds to the direct FA oxidation pathway. The potential of FA oxidation peaks on PdAu does not change or is slightly positively shifted relative to that on Pd/C. However, a wider potential window of FA oxidation can be seen on the PdAu/C catalysts. Similar effect observed on Au/Pd nanostructures [12,13] has been related to inhibited adsorption of hydroxyl groups on the PdAu relative to that on Pd. Since adsorbed hydroxyl species inhibit the FA oxidation, the lower hydroxyl surface coverage on PdAu generated more free active sites leading to promotion of activity within wider potential range.

As shown in Fig. 8, current densities on PdAu-0.1 and PdAu-0.35 catalysts with bulk Au content below that of Pd are higher compared to that on pure Pd/C. This effect can be seen for both series catalysts. The

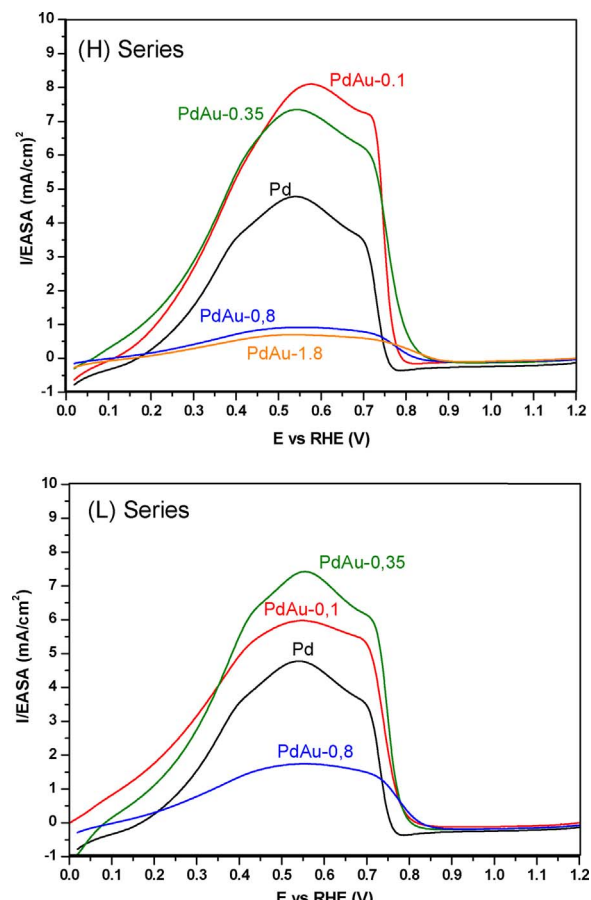


Fig. 8. Cyclic voltammograms of formic acid electrooxidation on Pd/C and bimetallic PdAu/C catalysts (Ar – saturated 0.5 M H₂SO₄ + 0.5 M FA solution, scan rate of 50 mV/s).

Pd-Au-0.1/C(H) catalyst with the lowest bulk Au content prepared in concentrated solution offers higher specific activity (8 mA/cm²) than its counterpart PdAu-0.1/C(L) prepared in diluted solution (6 mA/cm²). At higher bulk Au content, e.g. at Pd-Au-0.35 composition, current densities for series H and L catalysts are similar. However, when bulk contents of Au and Pd are comparable e.g. at Pd-Au-0.8 composition, the specific activity decreases, more on the H-series sample. Similarly low electroactivity is measured on the PdAu-1.8/C(H) catalyst with the highest Au-content.

The correlation between the PdAu composition and the electroactivity is further assessed by discussing the mass activity i.e. the peak current normalized to the Pd mass (mA mg_{Pd}⁻¹) and normalized to the total metal mass (mA mg_{Pd+Au}⁻¹) calculated at the E = 0.54 V [17,55,56].

Note that the Pd mass on the electrode was constant, 10 µg Pd/cm² whereas the content of Au increased. As shown in Fig. 9 a the activity normalized to the Pd mass on all the series L catalysts is higher compared to that on pure Pd/C. The activity of PdAu-0.1/C(L) catalyst (2097 mA mg_{Pd}⁻¹) is ca. 3-times higher compared to pure Pd (728 mA mg_{Pd}⁻¹) and with growing Au content the activity slowly decreases. On the other hand, among all series H samples, two catalysts PdAu-0.1 and PdAu-0.35 with lower bulk Au content exhibit activity higher than that of pure Pd whereas activity strongly decreases at higher bulk Au content. It clearly shows that in both series catalysts, the best performance toward the FA electrooxidation is obtained at the lowest Au-content, i.e. at PdAu-0.1 composition. Similar effect is observed when current density referred to the total mass of metals is discussed (Fig. 9 b). The activities measured on two catalysts with the lowest Au content, i.e. PdAu-0.1(L) and PdAu-0.1(H) catalysts are 2.4

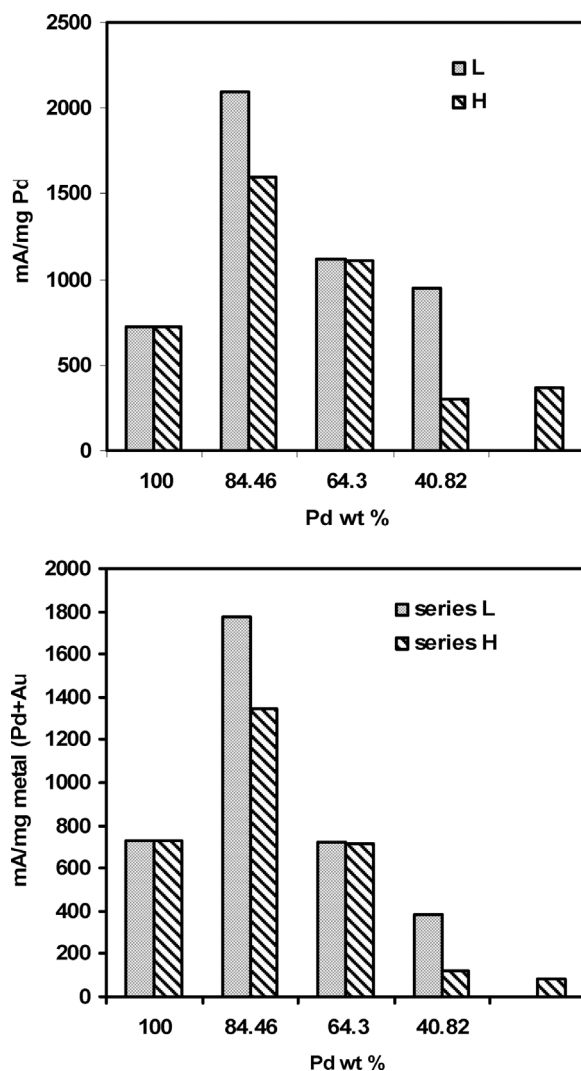


Fig. 9. Formic acid electrooxidation on PdAu/C catalysts in Ar-saturated 0.5 M H_2SO_4 + 0.5 M FA solution, scan rate of 50 mV/s. Current density at the 0.54 V (RHE) normalized to the Pd mass ($\text{mA mg}_{\text{Pd}}^{-1}$) and normalized to the total metal mass ($\text{mA mg}_{\text{Pd+Au}}^{-1}$) versus composition of bimetallic PdAu particle (wt% Pd).

and 1.8-times higher compared to that on pure Pd. At higher bulk Au content the mass activities normalized to the total metal mass are lower compared to pure Pd. Hence, electrochemical tests show that the PdAu catalysts with very low Au bulk content exhibits enhanced electroactivity towards FA oxidation compared with pure Pd catalyst.

The review paper published in 2015 compared electroactivity of various Pd-based catalysts (bulk metal, metal nanoparticles, metal nanostructures) towards FA electrooxidation [1]. The Pd-mass electroactivities on the catalysts with Pd particles on carbon-type supports were observed within a range from ca. 190 up to ca. 1400 $\text{mA mg}_{\text{Pd}}^{-1}$ (measured at the conditions 0.5 M H_2SO_4 /0.5 M FA/50 mV s⁻¹). In the FA oxidation on the 20% Pd/VC XC-72 catalysts current density of 193 [57] and 196 $\text{mA mg}_{\text{Pd}}^{-1}$ (EASA = 36.4 m²/g) [20] was reported. The oxidation of FA on 40% Pd/VC XC-72 catalyst generated current density of 212 $\text{mA mg}_{\text{Pd}}^{-1}$. These activity data were measured on catalysts with high Pd loading, 20–40 wt%. Xin et al. [58] reported that 30%Pd/C (commercial) shows current density of 211.4 $\text{mA mg}_{\text{Pd}}^{-1}$ (EASA 32.76 m²/g) whereas the catalysts with much lower Pd loading, i.e. 3.2 wt% Pd on modified CNT supports exhibit much better electroactivity, 371 (EASA 56 m²/g) and 695 $\text{mA mg}_{\text{Pd}}^{-1}$ (72 m²/g). In view of these activity data and essential role of the surface in catalysis the authors considered whether 20–30 wt% noble metal loadings are

required for significant FA oxidation and mechanistic studies [58]. In the catalysts studied in the present work palladium loading is low, equal to 2 wt% Pd. The catalyst with higher Pd loading, i.e. 10%Pd/VC XC-72 prepared by the same microemulsion procedure has been described in our previous work [59]. It characterized by the similar size of Pd particles (ca. 6.7 nm) and when tested in the FA electrooxidation reaction it generates current density of 414 $\text{mA mg}_{\text{Pd}}^{-1}$ (EASA 6.23 m²/g).

Metal dispersion (D, %) in all studied catalysts is similar, within 15–26% (Table 1). In order to compare a real activity of the active sites in studied PdAu catalysts, the values of turnover frequency (TOF) for the FA oxidation calculated according to Eq. (3) [60–62] are summarized in Table 1.

$$\text{TOF} = i_k/n e N_S \quad (3)$$

where i_k is the specific current density at potential of 0.54 V, n is the number of electrons transferred, e is elementary charge, N_S is atomic surface density. The values of TOF are calculated at the potential of 0.54 V (vs RHE) corresponding to the maximum current at pure Pd/C similarly to [59]. It is generally accepted that formic acid on Pd surface oxidizes solely through dehydrogenation path [1,2,6] and, consequently, $n = 2$ is assumed in the calculation.

As Au/C catalyst was inactive for FA oxidation, the Au could be considered as an inert additive. Therefore it could be assumed that the obtained values of TOF present in fact the reactivity of Pd sites in our PdAu/C catalysts.

However, the PdAu particles differ in the surface fraction of Au. In order to make easier further discussion, the calculated TOF values are given in Fig. 6 c. It can be seen that irrespective of the preparation procedure, when the surface fractions of Au are ca. 9–10% the values of TOF are comparable (17.03 s⁻¹ and 17.47 s⁻¹) and are ca. 1.5-times higher than that on Pd (11.36 s⁻¹). The values of TOF are smaller, 15.88 and 12.58 s⁻¹ at higher Au surface fraction (0.12 and 0.24) in the PdAu-0.35/C(2.5) and PdAu-0.8/C(R) catalysts, respectively, however, both are still higher than that on pure Pd.

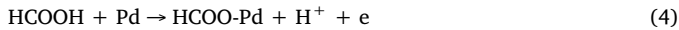
Thus, the most effective PdAu/C catalysts are those with alloy structure, i.e., with the Au surface fraction not higher than 0.09–0.1 which might be approximated by the Pd/Au ratio of 9/1. The active sites at this composition displays TOF values ca. 1.6 times higher than that on pure Pd surface. The TOF decreases at higher surface fraction of Au.

Thermal stability of this surface composition was also tested in separate experiments. The PdAu-0.35/C(H) catalyst was calcined at temperatures of 150, 250 and 400 °C for 2 h in Ar atmosphere. Fig. S 5 illustrates the thermal stability of the catalyst, by comparing the XRD patterns of fresh and calcined catalysts. This thermal treatment does not induce essential changes in the metal phase of PdAu-0.35 catalyst. The diffraction line of metal locates at the same positions as that in the fresh catalyst indicating that the PdAu alloy structure has been preserved. There is also no essential change in the shape of the diffraction line indicating well stability of the PdAu metal particles upon such temperature treatment. The samples of as-prepared and calcined catalysts were also tested in the hydrogenation of cinnamaldehyde with procedure described in our previous publication [32]. There was no change in activity and selectivity of reaction thus confirming thermal stability of this surface.

The effect of bimetallic PdAu structure on the FA dehydrogenation activity has been studied by DFT in quite recent work reported by Lee et al. [8]. FA dehydrogenation energy was calculated on four PdAu model alloys with varying surfaces and subsurface PdAu arrangements. Among them, the Pd3Au1 surface exhibited the lowest reaction energy and kinetic barrier for FA dehydrogenation. The triangular shaped Pd atoms played a critical role as they favorably stabilize the transition state (reaction intermediates). The energy barrier was the highest for the Au-rich surface with a single Pd atom completely surrounded by the

Au atoms. Furthermore, Bulushev et al. [35] observed 2–3 times lower activity of PdAu/Al₂O₃ catalysts (TOF) with the PdAu particles of alloy structure and surface composition close to the Pd₂Au compared to pure Pd in vapor phase FA decomposition. This effect has been explained by substitution of very active Pd surface sites like edge, corner by the Au atoms. The values of TOF (Fig. 6c, Table 1) calculated for the Au-rich catalysts are distinctly lower than that for pure Pd, whereas active sites in the particles with the surface Pd/Au ~9/1 composition are ca. 1.6-times more active compared to pure Pd. It is also observed that at somewhat higher Au surface fraction the activity decreases. The obtained surface Pd/Au ~9/1 composition is well supported by the recent studies dealing with the effect of the Pd surface content and its arrangement in the Pd₃Au catalyst for FA oxidation reaction [63]. It has been measured that FA electroactivity significantly increased (ca. 2.5-times) due to the CO-induced surface segregation leading to the higher surface Pd/Au ratio relative to the Pd₃Au initial one (Pd surface fraction grows from 67 up to 80%). These experimental data found confirmation in the DFT calculations showing that the increase of surface Pd content (> 75%) makes the FA oxidation more thermodynamically favorable. This effect has been related to the availability of the 3-fold hollow sites associated with one Au and two Pd atoms whose population decreases by increasing the Pd content on the alloy surface.

A volcano shape relation for FA electrooxidation vs the energy of the Pd d-band center reported by Hu et al. [64] on several Pd-based alloys (PdNi, PdCu, PdNiCu/C, PdAu) indicates that an optimum electron properties of the active Pd sites are required to reach the highest activity. This effect has been explained assuming that during the FA electrochemical oxidation on the Pd-sites, HCOO(ads) (HCOO-Pd) is first formed as a reactive intermediate via breaking the O–H bond in the HCOOH molecule [65,66]. Its decomposition to CO₂ proceeds through a transition state such as a tilted bridge-bonded configuration with two Pd–O bonds and a H atom approaching to the Pd site (Eq. (5)).



By shifting the Pd d-band center away from the Fermi level, the bond strength between intermediate species (HCOOads) and Pd becomes weaker. Consequently Pd–O bond dissociation is easier. However, as the d-band center further shifts away from its optimum value, the Pd–O bond becomes too weak resulting in the formation of less key intermediate species (HCOOads). Furthermore, the Pd–H bond (Eq. (5)) would become too weak as well, which makes the decomposition of HCOOads into CO₂ by breaking its C–H bond more difficult [64]. Thus, it can be seen from this mechanism, that the strength of Pd–H bonds which is determined by chemisorption ability of active sites should be also taken into consideration.

Furthermore, the presence of hydrogen accumulated by palladium was found to be crucial in the Pd-catalysed electroreduction of CO₂ yielding CO as a main product with small amounts of carbonyl-type by-products [67]. Although reactivity of Pd sites for the CO₂ electro-reduction correlated with the metal tendency toward CO₂ and intermediates species adsorption, the adsorbed H on the Pd surface was an essential requirement for the reaction [68]. The principal reaction pathway for CO₂ reduction in aqueous media involved reactions between CO₂(ads) and H_{ads} or H⁺ at hydrogen-evolution potentials. Hydrogen accumulated in bulk Pd electrode [69] or hydrogen inserted into Pd bulk electrode prior to the experiment [70] substantially enhanced Pd activity toward CO₂ electroreduction. All these observations clearly show that the presence of H(ads) enhances the CO₂ reduction [71,72]. Moreover, recently published DFT calculations have shown that accumulation of H atoms on the Pd(111) surface can accelerate deactivation of Pd by the CO species in FA decomposition [73].

The reverse water gas shift reaction (CO + H₂ → CO₂ + H₂) has

been suggested as the source of CO commonly observed in vapor-phase decomposition of FA on Pd-based catalysts [74]. At these conditions, reaction proceeded with the participation of two dissociatively adsorbed H species and the CO₂ intermediate-species with a weakened C=O bond due to adsorption on a metal surface [75]. It should be stressed that electroreduction of CO₂ formed via dehydrogenation of FA was found to be a main source of CO accumulated on the Pd surface [5–7].

The obtained CV profiles show that the strength of hydrogen bonding in the Au-containing particles is weaker than in bulk Pd. It is also observed that Au reduces ability of the Pd_{100-x}Au_x particles toward hydrogen accumulation which is almost completely suppressed at comparable Pd and Au bulk contents (Pd₅₆Au₄₄) in the PdAu-0.8/C catalyst. However, active sites in the latter catalyst exhibit relatively low activity (TOF) toward FA electrooxidation which could be ascribed to a too high Au-surface fraction [8]. The best surface arrangement of Pd and Au atoms expressed by the surface composition of Pd/Au ~9/1 in the PdAu-0.35/C catalyst gives 1.6-times higher TOF compared to pure Pd. However, at PdAu-0.35 composition, the hydrogen solubility is only partially reduced compared to pure Pd. Thus, a consequence of electronic modification of Pd by Au in the Pd_{100-x}Au_x particles is a change of the hydrogen solubility and the strength of the Pd–H bond. It seems, that apart from an appropriate surface Pd/Au arrangement required for enhancement of FA dehydrogenation rate also the Au-induced hydrogen related effects may affect catalytic performance of PdAu nanostructures for the FA electrooxidation reaction.

4. Conclusions

Two series of carbon-supported Pd_{100-x}Au_x catalysts of different Au contents have been synthesized by the “water-in-oil” microemulsion method using precursor solutions of low (series L) and high concentration (series H). The metal particles of low bulk Au-content (Au/Pd < 1) are of high monodispersity and of smaller size than their monometallic Pd and Au counterparts. At higher bulk Au-content (Au/Pd > 1), the particle size increases, gradually approaching almost the size of pure Au particles. A Pd-rich surface of all the Pd_{100-x}Au_x particles occurs, much pronounced in the series H catalysts prepared in solution of high precursors concentration. The high monodispersity of the metal particle size in the studied catalysts made it possible to observe a relation between the surface composition of the PdAu particles and activity for the FA electrooxidation. The catalytically active sites formed in the studied catalysts at the Au surface fraction ca. 0.1–0.12 (Pd 0.9–0.88) display the highest activity which is 1.6-times higher (TOF) as compared to pure Pd. It is also observed that higher surface fraction of Au strongly reduces activity. The occurrence of electronic modification of Pd by Au also results in a reduced hydrogen solubility, accompanied by weaker Pd–H bonds, which might influence the poisoning ability by CO formed through reduction of CO₂, product of FA electrooxidation.

Acknowledgements

The studies are partially supported by Marian Smoluchowski Krakow Research Consortium - Leading National Research Centre KNOW supported by Ministry of Science and Higher Education of Poland.

Appendix A. Supplementary data

Supplementary data associated with this article can be found, in the online version, at <http://dx.doi.org/10.1016/j.apcatb.2017.09.039>.

References

[1] H. Meng, D. Zeng, F. Xie, Catalysts 5 (2015) 1221–1274.

[2] R. Zhang, H. Liu, B. Wang, L. Ling, *J. Phys. Chem. C* 116 (2012) 22266–22280.

[3] X. Yu, P.G. Pickup, *J. Power Sources* 187 (2009) 493–499.

[4] M. Arenz, V. Stamenkovic, T. Schmidt, K. Wandelt, P.N. Ross, N.M. Markovic, *Phys. Chem. Chem. Phys.* 5 (2003) 4242–4249.

[5] J.-Y. Wang, H.-X. Zhang, K. Jiang, W.-B. Cai, *J. Am. Chem. Soc.* 133 (2011) 14876–14879.

[6] K. Jiang, H.-X. Zhang, S. Zou, W.-B. Cai, *Phys. Chem. Chem. Phys.* 16 (2014) 20360–20376.

[7] M.D. Obradovic, S. Ij. Gojkovic, *Electrochim. Acta* 88 (2013) 384–389.

[8] J.H. Lee, J. Cho, M. Jeon, M. Ridwan, H.S. Park, S.H. Choi, S.W. Nam, J. Han, T.-H. Lim, H. Ch Ham, Ch W. Yoon, *J. Mater. Chem. A* 4 (2016) 14141–14147.

[9] M. Wen, K. Mori, Y. Kuwahara, H. Yamashita, *ACS Energy Lett.* 2 (2017) 1–7.

[10] Z.-Li. Wang, J.-M. Yan, H.-Li Wang, Y. Ping, Q. Jiang, *J. Mater. Chem. A* 1 (2013) 12721–12725.

[11] K. Tedesree, T. Li, S. Jones, Ch W.A. Chan, K.M.K. Yu, P.A.J. Bagot, E.A. Marquis, G.D.W. Smith, S. Ch, E. Tsang, *Nature Nanotechnol.* 6 (2011) 302–307.

[12] Ch. Hsu, Ch. Huang, Y. Hao, F. Liu, *Electrochim. Comunn.* 23 (2012) 133–136.

[13] Ch. Hsu, Ch. Huang, Y. Hao, F. Liu, *J. Power Sources* 243 (2013) 343–349.

[14] W. Zhou, J.Y. Lee, *Electrochim. Commun.* 9 (2007) 1725–1729.

[15] C.H. Chen, W.J. Liou, H.M. Lin, S.H. Wu, A. Borodzinski, L. Stobinski, P. Kedzierszawski, *Fuel Cells* 10 (2010) 227–233.

[16] Y. Liu, L. Wang, G. Wang, Ch. Deng, B. Wu, Y. Gao, *J. Phys. Chem. C* 114 (2010) 21417–21422.

[17] Y. Suo, I.-M. Hsing, *Electrochim. Acta* 56 (2011) 2174–2183.

[18] Y.-H. Qin, Y. Jiang, D.-F. Niu, X.-S. Zhang, X.-G. Zhou, L. Niu, W.-K. Yuan, *J. Power Sources* 215 (2012) 130–134.

[19] G. Zhang, Y. Wang, X. Wang, Y. Chen, Y. Zhou, Y. Tang, L. Lu, J. Bao, T. Lu, *Appl. Catal. B* 102 (2011) 614–619.

[20] T. Maiyalagan, X. Wang, A. Manthiram, *RSC Adv.* 4 (2014) 4028–4033.

[21] S. Zhang, M. Qing, H. Zhang, Y. Tian, *Electrochim. Commun.* 11 (2009) 2249–2252.

[22] W.-Y. Yu, G.M. Mullen, D.W. Flaherty, C.B. Mullins, *J. Am. Chem. Soc.* 136 (2014) 11070–11078.

[23] D.W. Yuan, Z.R. Liu, *J. Power Sources* 224 (2013) 241–249.

[24] M.A. Lopez-Quintela, *Curr. Opin. Colloid Interface Sci.* 8 (2003) 137–144.

[25] M. Boutonnet, S. Logdberg, E.E. Svensson, *Current Opin. Colloid Interface Sci.* 13 (2008) 270–286.

[26] S. Eriksson, U. Nylen, S. Rojas, M. Boutonnet, *Appl. Catal. A* 265 (2004) 207–219.

[27] C. Tojo, D. Buceta, M.A. Lopez-Quintela, *Catalysts* 7 (2017) 68–85.

[28] C. Tojo, D. Buceta, M.A. Lopez-Quintela, *Nanoscale Res. Lett.* 10 (2015) 339–349.

[29] D. Buceta, C. Tojo, M.B. Vukmirovic, F.L. Deepak, A. Lopez-Quintela, *Langmuir* 31 (2015) 7435–7439.

[30] C. Tojo, M. de Dios, M.A. Lopez-Quintela, *J. Phys. Chem. C* 113 (2009) 19145–19154.

[31] Ming-Li Wu, D.-H. Chen, T-Ch Huang, *Langmuir* 17 (2001) 3877–3883.

[32] T. Szumel'da, A. Drelinkiewicz, R. Kosydar, J. Gurgul, *Appl. Catal. A* 487 (2014) 1–15.

[33] J. Long, H. Liu, S. Wu, S. Liao, Y. Li, *ACS Catal.* 3 (2013) 647–654.

[34] H. Kobayashi, M. Yamauchi, R. Ikeda, H. Kitagawa, *Chem. Commun.* (2009) 4806–4808.

[35] D.A. Bulushev, S. Beloshapkin, P.E. Plyusnin, Y.V. Shubin, V.I. Bukhtiyarov, S.V. Korenev, J.R.H. Ross, *J. Catal.* 299 (2013) 171–180.

[36] Ming-Li Wu, D.-H. Chen, T-Ch Huang, *Chem. Mater.* 13 (2001) 599–606.

[37] M.-Li. Wu, L.-B. Lai, *Colloids Surf. A* 244 (2004) 149–157.

[38] D. Chen, C. Chen, J. Mater. Chem. 12 (2002) 1557–1562.

[39] C. Tojo, M.C. Blanco, F. Rivadulla, M.A. Lopez-Quintela, *Langmuir* 13 (1997) 1970–1977.

[40] D. Chen, J. Yeh, T. Huang, *J. Colloid Interface Sci.* 215 (1999) 159–166.

[41] X. Zhang, K.Y. Chan, *Chem. Mater.* 15 (2003) 451–459.

[42] B. Barlett, H. Gollas, A. Duncan, *Electrochim. Acta* 53 (2008) 6845–6850.

[43] M. Łukaszewski, K. Kuśmierczyk, J. Kotowski, H. Siwek, A. Czerwinski, *J. Solid State Electrochem.* 7 (2003) 69–76.

[44] A. M.Łukaszewski, J. Czerwinski, *Solid State Electrochem.* 12 (2008) 1589–1598.

[45] M. Łukaszewski, A. Zurowski, M. Grdeń, A. Czerwinski, *Electrochim. Commun.* 9 (2007) 671–676.

[46] S. Hu, S. Ha, L. Scudiero, *Electrochim. Acta* 105 (2013) 362–370.

[47] H.-X. Zhang, Ch. Wang, J.-Y. Wang, J.-J. Zhai, W.-B. Cai, *J. Phys. Chem. C* 114 (2010) 6446–6451.

[48] L.A. Kibler, A.M. El-Aziz, R. Hoyer, D.M. Kolb, *Angew. Chem. Int. Ed.* 44 (2005) 2080–2084.

[49] A. Ruban, B. Hammer, P. Stoltze, H.L. Skriver, J.K. Norskov, *J. Mol. Catal. A* 115 (1997) 421.

[50] R. Patabiraman, *Appl. Catal. A* 153 (1997) 9–20.

[51] D.A.I. Rand, R. Woods, *J. Electroanal. Chem.* 36 (1972) 57–69.

[52] M. Simoes, S. Baranton, Ch. Coutanceau, *J. Phys. Chem. C* 113 (2009) 13369–13376.

[53] S. Lankiang, M. Chiwata, S. Baranton, H. Uchida, Ch. Coutanceau, *Electrochim. Acta* 182 (2015) 131–142.

[54] N. Toshima, T. Yonezawa, *New J. Chem.* (1998) 1179–1201.

[55] Z. Zhang, J. Ge, L. Ma, J. Liao, T. Lu, W. Xing, *Fuel Cells* 9 (2009) 114–120.

[56] R. Awasthi, R.N. Singh, *Int. J. Hydrogen Energy* 37 (2012) 2103–2110.

[57] J. Yang, Ch. Tian, L. Wang, H. Fu, *J. Mater. Chem.* 21 (2011) 3384–3390.

[58] Z. Xin, S. Wang, J. Wang, X. Huang, X. Ji, Y. Yao, L. Shao, *Electrochim. Commun.* 67 (2016) 26–30.

[59] M. Goral-Kurbiel, R. Kosydar, J. Gurgul, B. Dembinska, P.J. Kulesza, A. Drelinkiewicz, *Electrochim. Acta* 222 (2016) 1220–1233.

[60] B.S. Yeo, A.T. Bell, *J. Am. Chem. Soc.* 133 (2011) 5587–5593.

[61] L. Zhang, L. Wan, Y. Chen, Y. Zhou, Y. Tang, T. Lu, *Appl. Catal. B* 138–139 (2013) 229–235.

[62] U.A. Paulus, A. Wokaun, G.C. Scherer, T.J. Schmidt, V. Stamenkovic, V. Radmilovic, N.M. Markovic, P.N. Ross, *J. Phys. Chem. B* 106 (2002) 4181–4191.

[63] S.-Y. Lee, N. Jung, J. Cho, H.-Y. Park, J. Ryu, I. Jang, H.-J. Kim, E. Cho, Y.-H. Park, H. Ch Ham, J.H. Jang, S.J. Yoo, *ACS Catal.* 4 (2014) 2402–2408.

[64] S. Hu, F. Munoz, J. Noborikawa, J. Haan, L. Scudiero, *Appl. Catal. B* 180 (2016) 758–765.

[65] H. Miyake, T. Okada, G. Samjeske, M. Osawa, *Phys. Chem. Chem. Phys.* 10 (2008) 3662–3669.

[66] Y. Wang, Y. Qi, D. Zhang, Ch. Liu, *J. Phys. Chem. C* 118 (2014) 2067–2076.

[67] R.P.S. Chaplin, A.A. Wragg, *J. Appl. Electrochem.* 33 (2003) 1107–1123.

[68] S. Taguchi, A. Aramata, M. Enyo, *J. Electroanal. Chem.* 372 (1994) 161–168.

[69] K. Hashimoto, K. Ohkawa, A. Fujishima, *Proceedings of the Symposium on Environmental Aspects of Electrochemistry and Photoelectrochemistry* (1993) pp. 2209.

[70] W.M. Ayers, M. Farley, *J. Am. Chem. Soc.* 110 (1988) 147–153.

[71] M. Jitaru, D.A. Lowy, M. Toma, B.C. Toma, L. Oniciu, *J. Appl. Electrochem.* 27 (1997) 875–889.

[72] H. Siwek, M. Łukaszewski, A. Czerwinski, *Phys. Chem. Chem. Phys.* 10 (2008) 3752–3759.

[73] F. He, K. Li, G. Xie, Y. Wang, M. Jiao, H. Tang, *J. Power Sources* 316 (2016) 8–16.

[74] D.A. Bulushev, J.R.H. Ross, *Catal. Today* 163 (2011) 42–46.

[75] H.J. Freund, M.W. Roberts, *Sur. Sci. Rep.* 25 (1996) 225–273.